Hole-extraction and photostability enhancement in highly efficient inverted perovskite solar cells through carbon dot-based hybrid material

Daniele Benetti[a,1], Efat Jokar[b,d,1], Che-Hsun Yu[b], Amir Fathi[b], Haiguang Zhao[a], Alberto Vomiero[c,**], Eric Wei-Guang Diau[b,d,***], Federico Rosei[a,e,*]

[a] INRS Centre for Energy, Materials and Telecommunications, 1650 Boulevard Lionel-Boulet, Varennes, Québec, J3X 1S2, Canada
[b] Department of Applied Chemistry, Institute of Molecular Science and Center for Emergent Functional Matter Science, National Chiao Tung University, No.1001, Ta-Hsueh Rd, Hsinchu, 30010, Taiwan
[c] Department of Engineering Sciences and Mathematics, Luleå University of Technology, 981 87, Luleå, Sweden
[d] Center for Emergent Functional Matter Science, National Chiao Tung University, 1001 Ta-Hsueh Rd, Hsinchu, 30010, Taiwan
[e] Institute of Fundamental and Frontier Science, University of Electronic Science and Technology of China, Chengdu, China

ARTICLE INFO

Keywords:
Carbon dots
Charge transport layer
Perovskite solar cells
Downshifting layer
Hole transport layer

ABSTRACT

We report the effect of the integration of carbon dots (Cdots) in high-performance inverted planar-heterojunction (PHJ) perovskite solar cells (PSCs). We used Cdots to modify the hole-transport layer in planar PSC devices. By introducing Cdots on graphene oxide (GO) as hole-transporting layer, the efficiency of the PSC improved significantly from 14.7% in the case of bare GO to 16.2% of the best device with optimized Cdots content. When applying Cdots with an engineered absorption in the UV range as downshifting layer, the device performance was further improved, attaining a maximum PCE of 16.8% (+14%); the stability of the device was also enhanced of more than 20%. Kelvin probe force microscopy (KPFM) and cyclic voltammetry (CV) were employed to analyze the electronic band alignment at the interface between GO/Cdots and the perovskite film. Holes were extracted and transferred to the conductive substrate more efficiently in the presence of Cdots, thus delaying charge recombination. Photoluminescence (PL), transient PL decays and transient photovoltage (TPV) decays investigated the charge-transfer kinetics and proved the retardation of charge recombination. This work reveals an effective enhancement of the performance of planar PSCs by using Cdots/GO as hole transport material.

1. Introduction

The generation of electric power directly from solar radiation represents a promising opportunity to address the increasing demand for clean energy, while decreasing the environmental impact caused by excessive CO_2 emissions from fossil fuels. Solar energy is the most abundant renewable energy source and solar cells provide a convenient means to harvest it. Because of the costly fabrication and maintenance of conventional solar cells, such as those based on Si, a new generation of more cost-effective solar cells, the so-called third generation, is being investigated. Various materials systems and architectures have been proposed and realized, such as dye-sensitized solar cells (DSSC) [1–3], organic-polymer solar cells (OPV) [4,5], quantum-dot solar cells (QDSC) [6,7] and perovskite solar cells (PSC) [8–10]. To effectively compete with commercial silicon solar cells, a significantly increased efficiency, enduring stability and decreased price per watt of generated power are required.

Among various methods that have been developed, an efficient approach to enhance the performance of third-generation solar cells is to improve the charge extraction using a suitable charge-transport layer (CTL). There are mainly two kind of CTL: hole transport layer (HTL) and electron transport layer (ETL). An effective CTL increases the extraction of the photo-generated charge carriers from the absorbing layer while avoiding their recombination. Strategies to increase charge collection include the use of various metal oxides, organic polymers and small organic molecules [11–15]. Among them, carbon nanomaterials, such as carbon nanotubes (CNT) [16], fullerene [17] and graphene nanosheets [18], are interesting alternative CTL materials that have

* Corresponding author. INRS Centre for Energy, Materials and Telecommunications, 1650 Boulevard Lionel-Boulet, Varennes, Québec, J3X 1S2, Canada.,
** Corresponding author.
*** Corresponding author. Department of Applied Chemistry, Institute of Molecular Science and Center for Emergent Functional Matter Science, National Chiao Tung University, No.1001, Ta-Hsueh Rd, Hsinchu, 30010, Taiwan.
E-mail addresses: alberto.vomiero@ltu.se (A. Vomiero), diau@mail.nctu.edu.tw (E. Wei-Guang Diau), rosei@emt.inrs.ca (F. Rosei).
[1] These authors contributed equally to this work.

been successfully employed in various solar cells, such as DSSC [19,20], OPV [21,22] and PSC [23–27]. In general, carbon nanoallotropes possess intriguing opto-electronic properties that can improve the efficiency of solar cells.

The latest addition to the carbon nanomaterials family are carbon dots (Cdots) [28]. They are composed of discrete, quasi-spherical nanoparticles of size less than 10 nm. They have emerged as prospective competitors to conventional semiconductor quantum dots (QDs) and recently they have been proposed as possible CTL for solar cells [29,30]. Cdots are exclusively composed of non-toxic, earth abundant elements (C, N, H and O) and can be synthesized in large quantities via a simple hydrothermal or microwave approach [31]. Relative to conventional semiconducting QDs, their advantages include being non-toxic, cheap, chemically stable and simply prepared from abundant carbon-based feedstock [29].

Within third-generation solar cells, organic or inorganic halides having a perovskite (PSK) crystal structure represent an opportunity to develop high efficiency solar cells with solution processes at modest production cost. In less than a decade, their power conversion efficiency (PCE) increased from 10% to over 23% [32,33]. Their excellent optical properties and their facile fabrication resulted in a rapid growth in research and publications on this topic [8,34,35].

The planar inverted configuration is one of the most widely used configurations of PSC. In this architecture, the cell is commonly illuminated from the p-side, resulting in a structure glass/ITO/HTL/perovskite/ETL/metal which functions in a superstrate configuration [10]. In this layout, the HTL is critical for achieving high V_{oc} and overall high performance [21,32].

So far, most inverted solar cells have used (3,4-ethenedioxythiophene):poly(styrenesulfonate) (PEDOT:PSS) as HTL. Although PEDOT:PSS-based PSK solar cells have been reported with high efficiency, severe charge injection losses at the interface can limit the V_{oc} [33]. Furthermore, due to its acidity, hygroscopic properties and inhomogeneous electricity, devices based on PEDOT:PSS showed poor long-term stability. Various promising HTLs, such as NiO_x [34], MoO_3 [35], CuSCN [36], and others, have also been explored to fabricate efficient inverted PSK solar cells in the superstrate configuration. In general, all these HTLs showed good performance at the cost of long and complicated fabrication processes.

Graphene structures have been shown to be effective CTLs and transparent conductive electrodes in PSCs [36]. For example, graphene oxide (GO), a well-known derivative in the graphene family, was applied as a hole-transport layer in inverted planar-heterojunction (PHJ) PSC and yielded a PCE exceeding 12% [24,36]. Although GO is an efficient hole-extracting material, hole propagation on the oxygen groups limits the transfer of extracted holes and causes charge recombination. Even if reduced graphene oxide (rGO) can solve this problem, there remain issues that should be addressed: rGO requires protracted and complicated preparation and yields poor surface coverage; in GO-based devices the hole propagation from GO to the indium tin oxide (ITO) substrate is slow [25].

Cdots have been already employed as electron transport layer, or as additive in the perovskite layer itself showing promising results [37–39]. Recently it has been also studied theoretically their use as hole transport layer [40]. In this work, to overcome the limitations of the GO layer, we introduce fluorescent Cdots to form a homogeneous GO/Cdots HTL to develop high efficiency inverted PHJ PSCs. Based on our knowledge, this is the first report in which is highlighted experimentally the hole transport ability of the Cdots. Exploiting the excellent opto-electronic properties of Cdots [29], this work demonstrates that an optimal amount of Cdots in optimized proportion in a composite with GO nanosheets can significantly improve hole extraction from the perovskite film at the interface with GO/ITO. The addition of Cdots creates an intermediate energy level that shifts the GO work function, enabling an improved alignment of energy levels with the perovskite film. In this way, the holes can be extracted more efficiently than from GO alone. The increased hole-transport property at the interface of ITO/GO/PSK increases the short-circuit current density (J_{SC}) and open-circuit voltages (V_{OC}), yielding a maximum efficiency of 16.2%, as opposed to a PCE of 14.7% obtained from the GO-based perovskite device.

Long term stability is one of the most critical parameters for solar cells in general (also because it affects overall cost), and is a major challenge for PSCs specifically. In particular, the stability of PSC under ultraviolet light remains a major problem [41,42]. To address this issue, we prepared UV-absorbing Cdots and embedded them in a polymer matrix to serve as the downshifting layer over the perovskite cell. The incorporation of Cdots as a protective layer increases the light-soaking stability by more than 20% and further increases the PCE of the solar cell to 16.8%.

2. Results and discussion

A solvothermal approach was employed to form Cdots with abundant functional groups, including hydroxyl, carboxyl and amide groups. These functional groups confer great dispersibility in polar solvents, such as water and methanol [43]. To integrate the Cdots in the PSC device, they must be compatible with the fabrication process; in particular they should be soluble in non-polar solvents such as hexane or slightly polar solvents, such as chlorobenzene and toluene. To obtain a non-polar solubility of the Cdots, the as synthesized Cdots were modified with oleylamine (OLA) according to our previous work [43]. In this procedure, an additional step to modify the surface was added to transfer them from a polar solvent to a non-polar solvent. By employing (1-Ethyl-3-(3-dimethylaminopropyl)carbodiimide, EDC), the primary amine from long carbon-chain molecule OLA reacted with the carboxyl group on the surface of the Cdots. The obtained OLA-modified Cdots exhibit hydrophobic features due to the long carbon chain, and can be efficiently dispersed in slightly polar solvents, such as chlorobenzene, and even in a non-polar solvent such as hexane. X-ray photoelectron spectroscopy (XPS) was carried out to evaluate the chemical composition of the Cdots (Fig. S1). From this analysis the presence of C, N and O is evident. The C 1s spectrum could be fitted with three Gaussian peaks with maxima located at 284.6, 286.8, and 288.1 eV, assigned to C–C (sp_3-hybridized), C–O/C–N, and O = C–O chemical states, respectively [44]. The high resolution N 1s band can be deconvolved into three main peaks corresponding to pyridinic (398.7 eV), pyrrolic (400.6 eV), and graphitic (402.1 eV) nitrogen atoms [45,46]. The O 1s band contains two main peaks at 531.7 and 532.1 eV for C = O and C–O, respectively [44].

Fig. 1 shows absorption and PL spectra of Cdots, before and after surface treatments with OLA (MeOH_Cdots and CB_Cdots respectively). The spectrum acquired from freshly synthesized Cdots exhibits strong absorption extending over the entire window of the visible wavelengths (300–700 nm); Fig. 1b and c report the 2D excitation-emission properties of the Cdots. As expected, the Cdots present wavelength-dependent emissions. The optical properties of the pristine Cdots are mainly preserved upon functionalization with OLA; absorption and emission bands are similar in both samples. The small differences are attributed to the solvents, as Cdots can exhibit a solvent-dependent shift, as previously reported [47]. The functionalization leaves the overall electronic properties of Cdots almost intact, while conferring on them an enhanced solubility in non-polar solvents.

To verify that the Cdots can inject holes in the GO, we carried out PL experiments. The solutions of Cdots with varied GO concentration were analyzed and the recorded PL spectra are displayed in Fig. 2. The substantial quenching indicates a strong interaction between Cdots and GO. The PL spectra in Fig. 2 show a dominant emission (maxima at 520 nm and 630 nm, when excited at 400 nm and 540 nm, respectively) for pure Cdots, whereas ~60% of the Cdots PL intensity is quenched by GO. In particular, the PL intensity decreases greatly with increasing concentration of GO in solution, while the position and shape of the

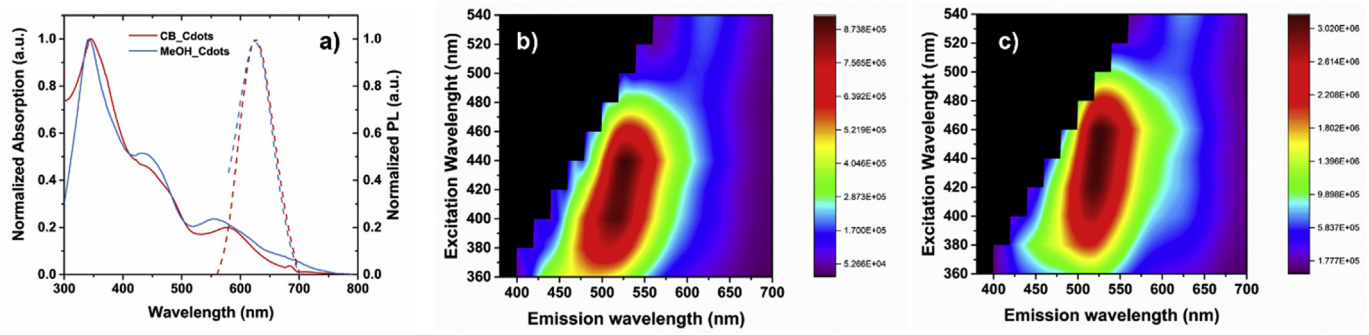

Fig. 1. a) Absorption and emission (λ_{ex} = 540 nm) of Cdots after purification (MeOH_Cdots, solvent is methanol) and after ligand exchange (CB_CDots, solvent chlorobenzene); b) 2D contour plot showing the wavelength-dependent emission of Cdots as synthesized (MeOH_Cdots); c) after ligand exchange and dispersed in chlorobenzene (CB_Cdots).

absorption lines are unaffected. As already reported in similar systems, this interaction can be ascribed to charge transfer of the photoinduced charge carriers in the Cdots to GO [47,48].

The Cdots/GO HTL was prepared by spin-coating the Cdots_CB dispersion solution of varied concentration (0.025, 0.05 and 0.1 mg/mL) over the GO layer. The surface morphology of the GO film with and without Cdots was analyzed by atomic force microscopy (AFM). The GO film (Fig. 2c) exhibits a nanosheet feature with 1–3 layers; the thickness is estimated to be ~2–3 nm. Cdots on the surface of GO are clearly observed (Fig. 2d), their size is in the range 4–6 nm and their presence does not alter significantly the RMS roughness (RMS ~1 nm vs 0.89 nm for the pure GO film).

The prepared GO/Cdots layer was used as HTL in an inverted PSC based on device configuration ITO/GO/Cdots/$MAPbI_3$/PCBM/Bathocuproine (BCP)/Ag (Fig. 3); a cross sectional scanning electron microscope (SEM) micrograph is shown in Fig. S2, ESI. Fig. S3, ESI, shows top-view SEM images for all perovskite films grown on ITO/GO and ITO/GO/Cdots substrates. Pinhole-free, close-packed and uniform perovskite films were formed, which are an essential condition for a high-performance solar cell in a planar structure [23]. The crystal structure of the perovskite film for all samples, ITO/GO and ITO/GO/Cdots, was analyzed using XRD; no significant variation of crystallinity

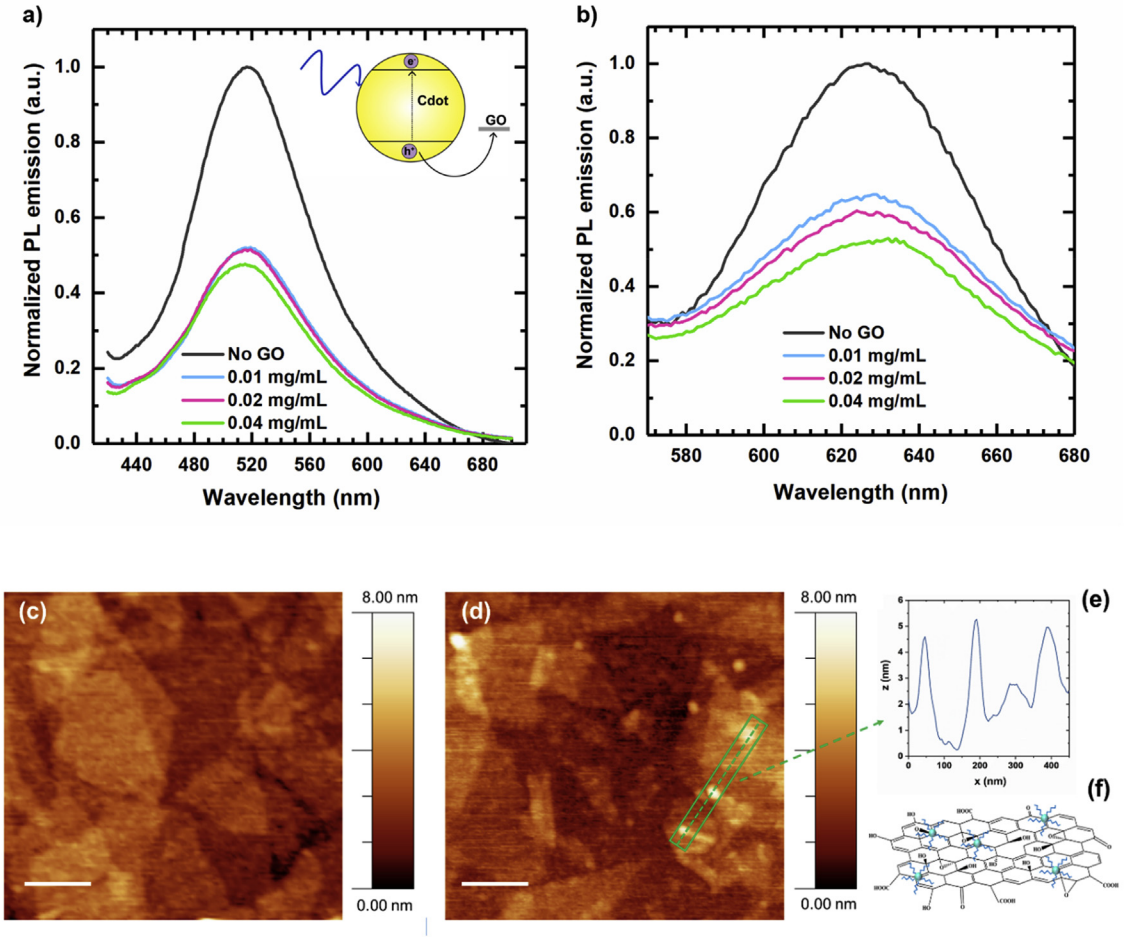

Fig. 2. Fluorescence spectra of Cdots in chlorobenzene solution at varied concentration of GO. a) λ_{ex} = 400 nm, b) λ_{ex} = 540 nm. Surface morphology of GO film (c), GO/Cdots (d) on area 1 μm × 1 μm. Cdots are clearly visible on the surface of the GO nanosheets. The scale bar is 200 nm. (e) depth profile of an assigned part and (f) schematic of graphene oxide nanosheets with Cdots deposited on top.

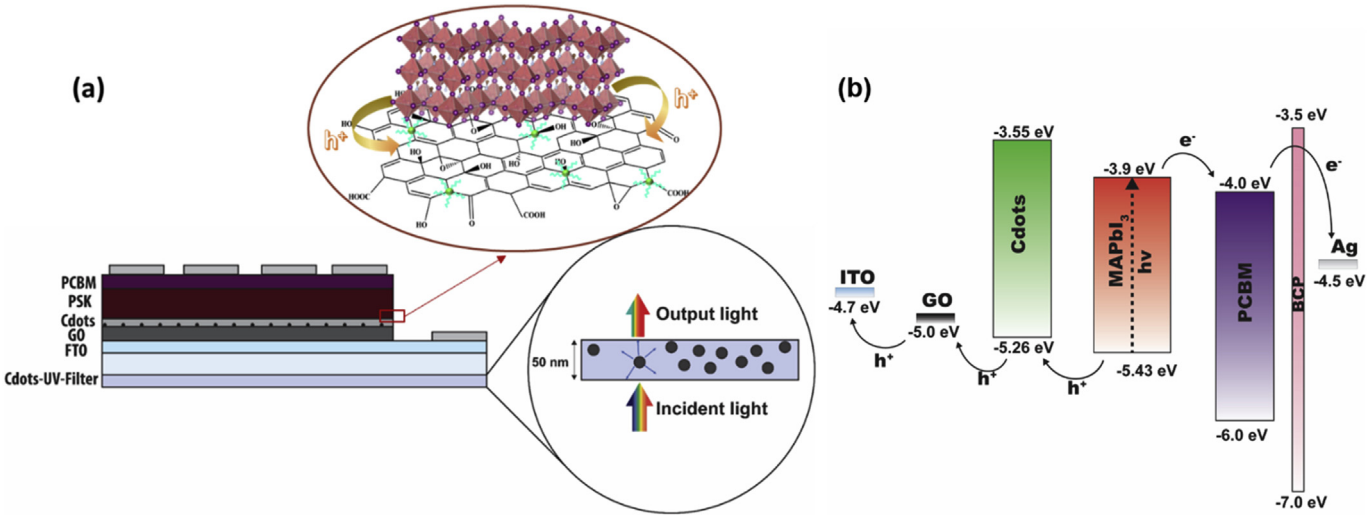

Fig. 3. a) Schematic of an inverted planar device with Cdots incorporated at the interface between GO and perovskite, and a protective/down-shifting layer made of Cdot/PVP on the exterior side; b) energy diagram of the perovskite cell (the energy values are reported vs Vacuum Level).

of the perovskite was observed (Fig. S4). In the inverted configuration, it is essential to have a transparent HTL so as not to lose the incident light and photocurrent. As shown in Fig. S5, the addition of Cdots does not increase the absorption in the 400–500 nm range, with no detrimental effect on the absorption of the perovskite layer. Hence, we can conclude that the improved performance of the devices arises from the changes of the optical and electronic properties at interface, as discussed below.

The effect of varied Cdots loadings on the functional properties of PSCs was investigated. The *J–V* curves of the best cells with varied concentration of Cdots in the GO/Cdots layer as HTL under AM 1.5G simulated sunlight and the efficiencies of incident photons to current (IPCE) are reported in Fig. 4. Table 1 reports the photovoltaic (PV) performance parameters (open-circuit voltage (V_{OC}), short-circuit current (J_{SC}), fill factor (FF) and PCE).

For the GO device, a PCE of 14.7% was obtained, a higher value compare to the one reported by Wu et al. (PCE = 12.4%) for a similar device [36]. In general, all the champion devices with GO/Cdots as HTL showed far superior PV performances: 15.6%, 16.2% and 15.4% for Cdots loading at 0.025, 0.05 and 0.1 mg/mL, respectively. The improved performances of GO/Cdots are due mainly to their increased J_{sc}. Higher short circuit current densities in GO/Cdots devices were confirmed by the IPCE spectra (Fig. 4b). The calculated J_{sc} values from the IPCE spectra are consistent with the J_{sc} values obtained from the *J–V* curve measurements. All the devices with Cdots show IPCE spectral features similar to those of the GO device, but with increased values in the entire wavelength range. Because of the weak absorption of Cdots relative to the perovskite film (Fig. S5), a significant contribution of Cdots to the light harvesting of the perovskite films can be excluded.

The effect of introducing Cdots in a GO layer as HTL is clearly discernible in the statistical data. Twenty devices were fabricated under the same experimental conditions for devices based on GO and GO/Cdots (with varied Cdots concentration); the corresponding PV parameters are listed in Tables S1–S4.

Fig. 4 c-f compares the J_{sc}, V_{oc}, FF and PCE distributions of these results with various hole extraction layers, giving mean PCE (%) = 13.4 ± 0.7, 14.3 ± 0.7, 14.9 ± 0.7 and 11.9 ± 1.2 for devices made of GO, GO/Cdots 0.025, GO/Cdots 0.05 and GO/Cdots 0.1, respectively. At the optimum amount of 0.05 mg/mL of Cdots on GO, all the functional parameters (V_{oc}, J_{sc}, FF and PCE) show the highest values. In general, GO/Cdots 0.1 devices present the lowest values among the Cdot-based PSC, due to the poor wettability of the perovskite solution on the surface of the GO/Cdots; this condition can also explain the large variation from the best value for this dataset. The poor wettability is confirmed by contact angle measurements (Fig. S6). By increasing the amount of non-polar Cdots deposited on GO, the hydrophobicity of the layer increases (higher contact angle), making more difficult the deposition of uniform perovskite films prepared by spin coating technique.

From these observations, we deduced that the addition of Cdots at an optimum amount on GO nanosheets increases the hole-extraction ability of the GO layer. To acquire further understanding of the mechanisms for the enhanced PCE, PL decay lifetimes and transient photovoltage (TPV) decays were measured. To elucidate the dynamics of charge-transfer processes at the GO/Cdots composite layer, we applied steady-state PL and transient PL decays with time-correlated single-photon counting (TCSPC) techniques; the results for representative samples are depicted in Fig. 5. Samples were prepared with a perovskite layer deposited on either an ITO/GO or an ITO/GO/Cdots layer while an ITO/PSK sample served as reference. All samples presented the characteristic perovskite excitonic emission feature centered at about 770 nm (Fig. 5a). When GO or GO/Cdots were introduced at the interface of the PSK layer, a strong PL quenching was observed, maximized at 0.05 mg/mL Cdots concentration with the PL intensities following the order ITO/PSK > ITO/GO/PSK > ITO/GO/Cdots_0.025/PSK > ITO/GO/Cdots_0.05/PSK. The steady-state PL quenching indicates a substantial contribution of Cdots to hole extraction from the perovskite film.

For a more direct confirmation of the Cdots role in the charge transfer, the PL lifetime was measured by TCSPC technique. Normalized transient PL decays of the corresponding samples (λ_{ex} = 635 nm, λ_{em} = 770 nm) are shown in Fig. 5b. A similar trend to the steady-state PL is observed, with the shortest decay being associated with the sample with GO/Cdots at 0.05 mg/mL. All PL transients were fitted with a bi-exponential decay model; the corresponding lifetimes and relative amplitudes are summarized in Table S5.

In general, for perovskite films fitted with a bi-exponential function, the first decay component corresponds to a non-radiative relaxation of the surface state in the grain boundaries of the perovskite while the second decay component is assigned to recombination events in the bulk [49]. The sample with 0.05 mg/mL Cdots contents has the smallest τ_1, 25 ns, compared with the GO sample, 46 ns. This data supports the hypothesis of an enhanced charge transfer in the presence of an optimal amount of Cdots.

To increase our understanding of the effect of Cdots on the hole-extraction mechanism in complete devices, we measured the TPV,

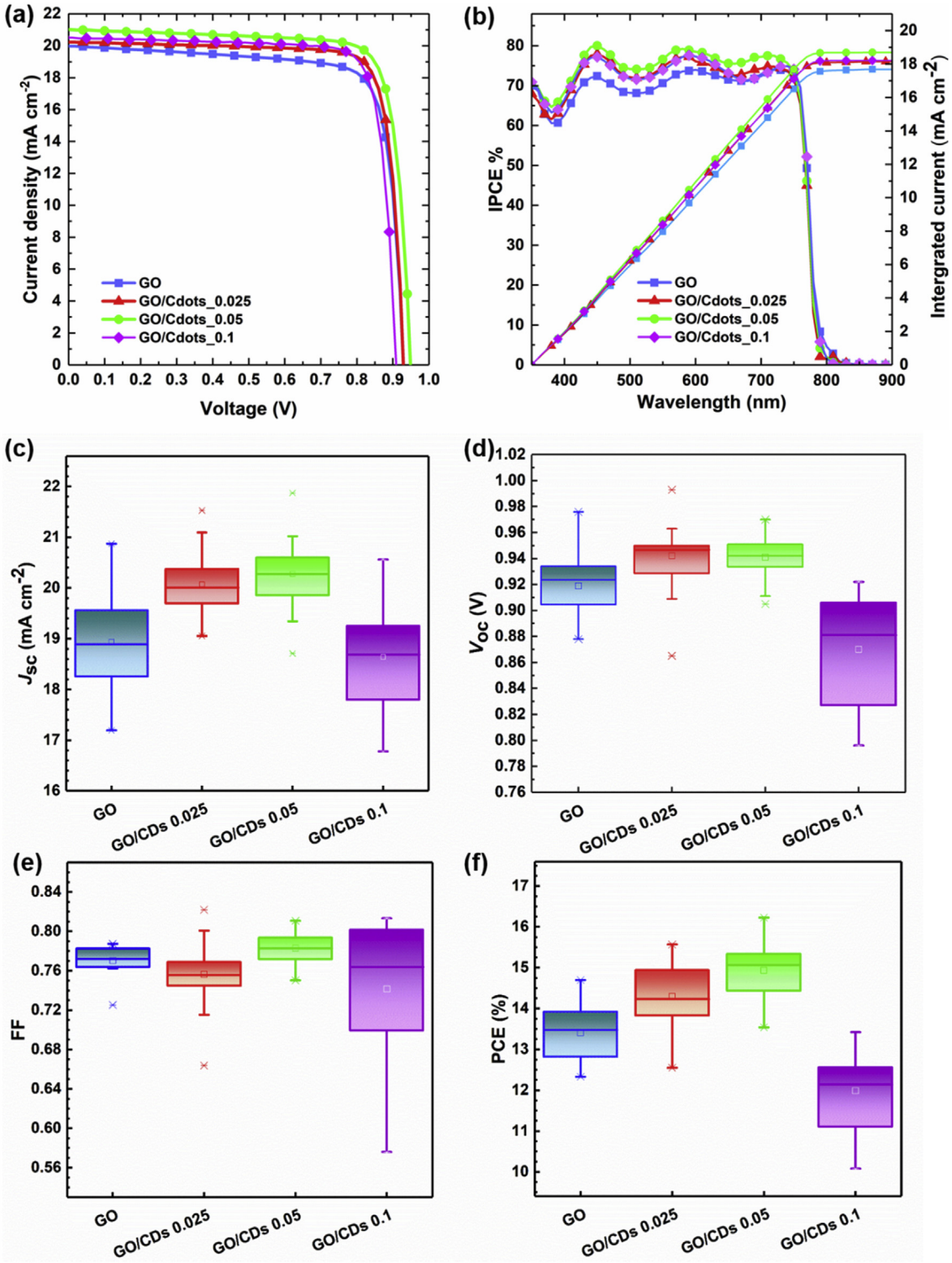

Fig. 4. a) *J-V* curves for the best samples under optmized conditions; b) IPCE and integrated current densities; c-f) Statistical box plots of photovoltaic parameters for inverted perovskite solar cells with Cdots at varied concentration on GO as HTL. For cells of each type, the fabrication was done under the same experimental conditions. Top and bottom of the boxes is the 75–25 percentile and the cross symbols represent outliers in box plot.

which is a measure of the rate of carrier recombination within the cells. In the TPV measurements, to achieve a steady-state equilibrium the solar cell was first illuminated under a white light bias, then a weak laser pulse was applied to generate an additional amount of charges in the devices. The transient open-circuit photovoltage associated with the charge population perturbation was then monitored to study the charge recombination processes. All photovoltage decay profiles were fitted with a single-exponential decay model; the values of the decay coefficient (τ_{rec}) for charge recombination are shown in Fig. 6. The rate of recombination of the carriers is proportional to the inverse of the decay lifetime; a longer lifetime hence indicates less recombination inside the device [50]. An increase in charge-recombination lifetime can be observed for all the cells incorporating the Cdots. In particular the cell with the optimum content of Cdots, GO/Cdots_0.05, showed the longest

Table 1
Photovoltaic parameters for the best devices containing three different amounts of Cdots, as well as the reference device.

Devices	J_{sc} (mA cm^{-2})	Integrated J_{sc} (mA cm^{-2})	V_{oc} (mV)	FF	PCE (%)
GO	20.0	17.7	935	0.787	14.7 (13.4 ± 0.7)
GO/Cdots 0.025	20.2	18.15	935	0.822	15.6 (14.3 ± 0.7)
GO/Cdots 0.05	21.0	18.7	953	0.801	16.2(14.9 ± 0.7)
GO/Cdots 0.1	20.6	18.2	922	0.810	15.4(11.9 ± 1.2)

lifetimes, indicating that a lower charge recombination rate was achieved. The TPV results suggest that a more favorable energy level alignment and good electron blocking capability of the hybrid GO/Cdots_0.05 hole transport layer could effectively suppress the charge recombination process.

Electrochemical impedance spectroscopy (EIS) served to elucidate the electronic properties and interfacial recombination in the solar cell with Cdots in varied amounts (Fig. 6b). For all samples, only one large semicircle is visible in the Nyquist plot; this arc, typically observed at medium frequencies, is related to the charge recombination inside the solar cell [51,52].

Generally, two semicircles can be observed. However in a high conductivity case (as in this case), in which either one of the transport resistances for electrons or holes is negligible, the geometric arc will not appear in the IS spectra in the high frequency region [51]. The most remarkable feature in the Nyquist plots is that the cell treated with 0.05 mg/mL Cdots leads to the larger arc indicating a reduced recombination phenomena. This is in agreement with the J-V measurement that showed a highest efficiency for this cell.

In particular, the response at different bias (V_{bias}) can be fitted to the simple circuit shown in Fig. S7 [50,51]. For the reason aforementioned, the model employed will not take into account the geometric capacitance. In addition, fitting the semicircle with a simple model containing only the series resistance (R_s), the recombination resistance (R_{rec}), and a capacitance (C_μ, chemical capacitance) gave a good fit and showed identical trends in the recombination resistance.

A further confirmation of the reduced recombination phenomena for the optimum amount of Cdots, comes from the analysis of R_{rec} when varying the voltage bias (Fig. 6c). In all the range of V_{bias}, the value of R_{rec} for the best cell (with 0.05 mg/mL Cdots) is higher compared to the others. The value of R_{rec} is inversely proportional to the charge recombination rate, so a higher value implies a significant suppression of the recombination rate. As the cells differ only for the HTL, we can attribute the reduced recombination to a better injection of holes in the ITO with a notable increment in the final PCE (as seen in the J-V analysis).

Introducing Cdots increased the charge recombination resistance, in agreement with the TPV results.

The presence of a hole-transfer potential barrier between the perovskite and GO interface was previously established [25]. Based on all PL decay, TPV measurements and EIS, we conclude that the addition of Cdots into the GO HTL enhances the electronic coupling for efficient mediation of the hole transfer from the perovskite to the ITO front contact, decreasing the recombination at this interface, and consequently increasing J_{SC}.

To improve the understanding of the actual role of Cdots on GO nanosheets, we evaluated the band diagram of the Cdots using cyclic voltammetry (CV) (Fig. S8). The measurements were performed at ~23 °C under inert atmosphere with a three-electrode system consisting of a Pt foil as the counter electrode, Cdots deposited on Au disk as working electrode and Ag/AgCl as reference electrode. The band positions of the Cdots were obtained from the onset oxidation potential (E_{ox}) and the onset reduction potential (E_{red}) with the equations reported in the experimental section. The HOMO and LUMO of Cdots were found to be −5.26 eV vs Vacuum Level and −3.55 eV vs Vacuum Level (Fig. 3b), respectively. The band position alignment of the Cdots supports the hypothesis of an improved hole transfer from the perovskite layer to the GO and their ability to provide band bending and shifting the GO work function downward towards more negative values, as reported in Fig. 6c. KPFM imaging supports this hypothesis: a shift of the contact potential difference towards less positive values was observed when the measurement was performed on a Cdot/GO sample. (Fig. S9). In the KPFM system employed, the potential was applied on the tip, meaning that CPD = ϕ_{tip}-ϕ_{sample}. A shift towards less positive values of the CPD, considering that the work function of the tip does not vary, means that the work function of the sample increased [53].

To confirm the band position of Cdots, we conducted tests with Cdots and PCBM. PCBM has HOMO/LUMO energies of −6.0 eV vs Vacuum Level and −4.0 eV vs Vacuum Level, respectively. In theory, Cdots, with a LUMO energy of – 3.55 eV vs Vacuum Level, would inject

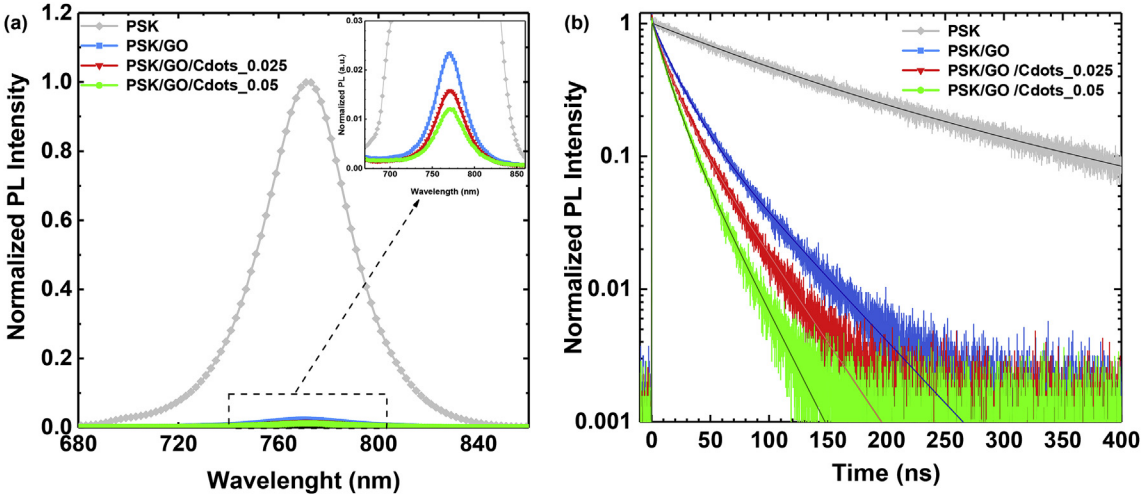

Fig. 5. a) Steady-state photoluminescence spectra of perovskite thin films deposited on ITO, on GO and on GO/Cdots with varied loading, collected with excitation λ_{exc} = 635 nm; b) transient PL decays obtained using the TCSPC technique with excitation at 635 nm and probe at 770 nm.

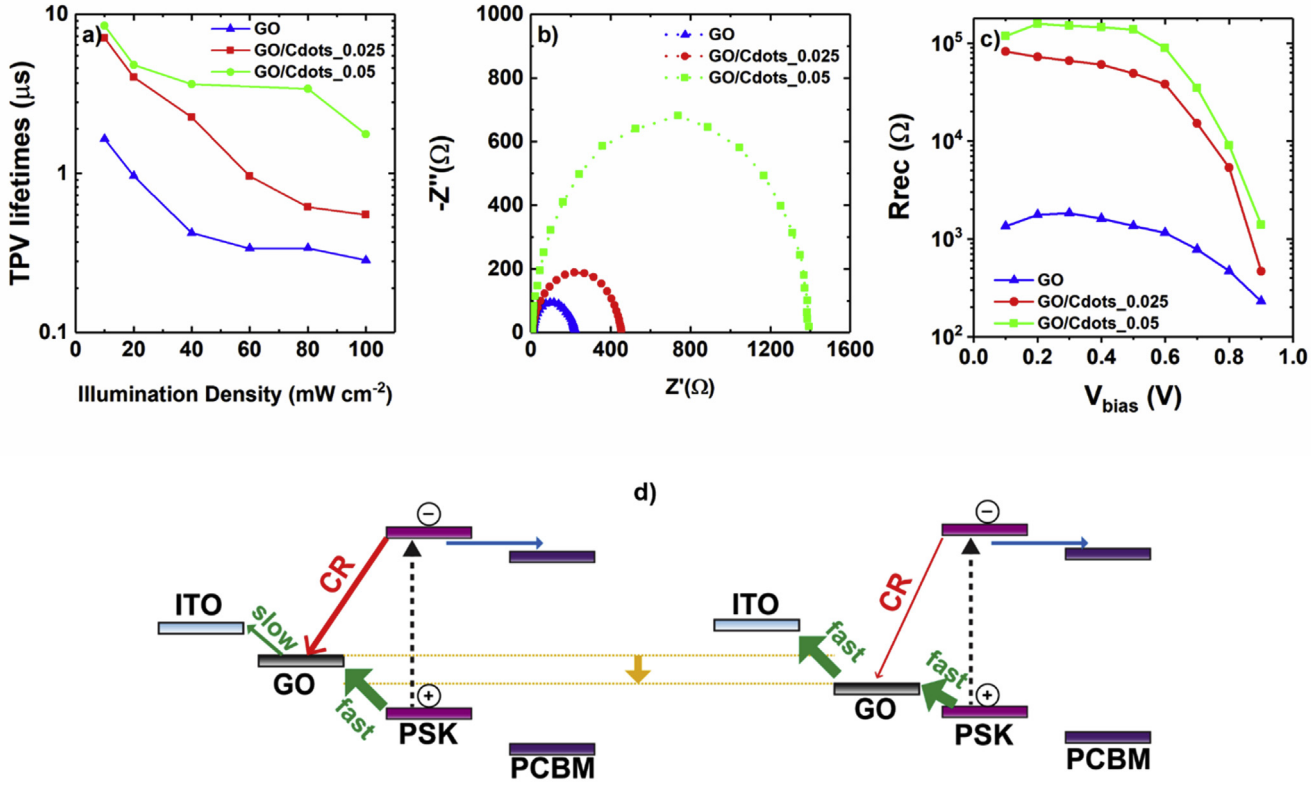

Fig. 6. a) Transient photovoltage measurement of representative samples at varied illumination densities; b) Nyquist plot at 900 mV in dark of three representative samples with varied HTL: GO, GO/Cdots_0.025 and GO/Cdots_0.05; c) recombination resistance of the three representative samples; (d) schematic illustration of a mechanism of charge transfer and charge recombination (CR) for GO and GO/Cdots to rationalize the observed hole-extraction kinetics at the HTL/PSK interface and the corresponding photovoltaic performance.

carriers into the PCBM layer, but they would create a barrier for the electrons from the perovskite to the electron-transport layer as their LUMO level is less negative than the one of the PSC layer (see Fig. S10). Fig. S11 reports the steady-state PL of a solution of Cdots with added PCBM; as expected, when PCBM was added, the emission was quenched. A solar cell was then assembled with a layer of Cdots deposited over the perovskite layer and covered with PCBM. As reported in Fig. S12, the short-circuit current of the cell decreases, yielding a PCE of 7.0%, confirming the barrier effect of the Cdots between the PSK layer and the PCBM.

An important aspect for the commercialization of perovskite-based devices is their long-term stability. The performance as a function of storage duration for two devices, GO and GO/Cdots, was measured for 1200 h at 25 °C and relative humidity 25–30% with no encapsulation; the results are reported in Fig. S13. Both devices maintained almost 90% of their initial efficiencies after storage for 1200 h, indicating the excellent stability of the GO-based devices relative to an organic HTL material such as PEDOT:PSS [25] . Another challenge related to the stability of PSCs is the stability of perovskite to ultraviolet light [8,41,42]. To address this condition and to increase the long-term stability of our devices, we exploited the unique optical properties of Cdots. As mentioned before, the optical properties of Cdots can be tuned through the preparation method: in this case, a different type of Cdots was synthesized with the same precursors using a microwave method. This batch of Cdots presented strong down-converting properties, with absorption in the UV region (see Fig. S14 and Fig. S15 for optical and chemical characterization) and emission around 450 nm. In this way, the photons in the UV region of Sun spectrum can be absorbed, removing the soaking effect on the perovskite film, re-emitted in the visible spectral region (max emission in the 450–500 nm region), and photoconverted into electric power. Cdots dispersed in isopropanol were subsequently mixed with polyvinylpyrrolidone (PVP) and spin-coated on the glass side of the PSC devices. Adding the protective layer of Cdots not only improved the stability of the device but also increased the PCE of the cell; the Cdots film acts, in fact, also as UV-to-Vis downshifting layer (DSL). The DSL absorbed the UV part of the sun spectrum and downshifted it to a more suitable range of wavelengths that can be absorbed by the perovskite film. This synergistic effect is clearly observed in the device, as shown in Fig. 7. The presence of an external thin film of Cdots increased J_{sc} by 3.8%, increasing the final PCE to 16.8%. The enhancement of the J_{sc} due to the effect of the downshifting of the UV light, is confirmed by the IPCE, in which the efficiency of photons to electrons in the range 350–500 nm is increased (Fig. 7b). To verify the light-soaking stability, we maintained the devices with or without the UV-to-Vis DSL under illumination at 1 sun without capsulation in an ambient condition (RH = 45–50%, T = 25 °C) (Fig. 7c). The device with the Cdots layer as UV-to-Vis DSL exhibited increased UV stability. The normalized PCE retained more than 62% of the initial PCE after 30 min of continuous operation under full irradiation. In contrast, the stability of the solar cell without a protective layer decreased to 48% of the initial PCE under the same testing conditions.

3. Conclusions and perspectives

In summary, we demonstrated a rapid and highly reproducible method to prepare an efficient and stable HTL for planar-heterojunction PSCs. The HTL was based on Cdots/GO. Our results show that the use of Cdots at an optimum amount improved the PCE of the device to 16.2%. In the reference cell containing only GO, the transfer of the localized holes into the ITO surface can be a bottleneck that increases the recombination at the PSK/GO interface. As evidence shown via PL

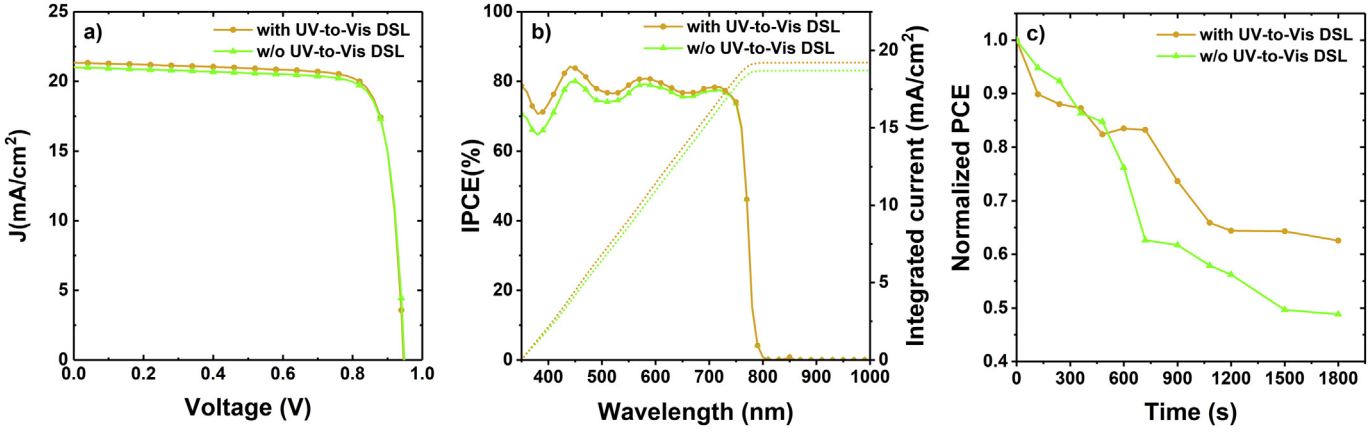

Fig. 7. a) *J-V* curve of the best samples with GO/Cdots 0.05 as HTL and with or without an external protective UV-to-Vis DSL; b) corresponding IPCE and integrated curves; c) light-soaking stability for the two samples.

lifetime decay, TPV decay, EIS, CV and KPFM, the addition of the Cdots shifted down the work function of GO, increasing the rate of hole injection and decreasing charge recombination so that the collection of photogenerated charges improved significantly. Moreover, employing appropriate UV-absorbing Cdots as a protective film on the exterior side of the PSC improved the stability against UV radiation by more than 20%; the PCE increased to 16.8%. The present work provides important indications for further investigation in exploiting the properties of carbonaceous nanomaterials as high-conductive CTL alternatives for improving the efficiency of planar PSCs. Moreover, the versatility of the Cdots shown here, with their environmental friendliness, non-toxicity, low-cost fabrication, and easily scalable production, can represent a practical and low-cost way to realize highly stable and efficient PSC.

4. Methods

4.1. Synthesis of carbon dots

Cdots were synthesized via a solvothermal method with citrate and urea as precursors, following previous work [43]. Citric acid (1 g) and urea (2 g) were typically dissolved in 10 mL of dimethylformamide (DMF) under stirring. When all precursors were dissolved, the transparent solution was transferred into an autoclave (volume 30 mL); the reaction proceeded for 6 h at 160 °C. After natural cooling to ~23 °C, the mixture was added dropwise to hexane (50 mL) to precipitate the Cdots. The precipitates were collected and dispersed in methanol (60 mL, MeOH_Cdots). For Cdots modified with oleylamine (OLA) - OLA-modified C-dots, MeOH_Cdots (5 mL) were added to 1-ethyl-3-(3-dimethylaminopropyl)carbodiimide (EDC) (250 mg) and OLA (1 mL). The mixture was stirred for at least 15 h near ~23 °C. After the reaction, additional hexane (20 mL) was mixed with the solution. The OLA-modified Cdots were transferred into the hexane phase after standing for 5 min. For purification of the OLA-modified C-dots, the product was kept at −10 °C for 1 h; at that temperature, the residual OLA precipitated and was removed. The OLA-modified Cdots were then dried at 70 °C in a vacuum oven and redispersed in chlorobenzene (CB_Cdots)

We used a different approach for the synthesis of optical UV absorbing Cdots [54]: citric acid (3.0 g) and urea (1.5 g) were dissolved in water (10 mL) under stirring. The precursors were subsequently placed in a microwave oven for 4 min; the obtained green slurry was dried in a vacuum oven at 60 °C. The obtained powder was dispersed in isopropyl alcohol and centrifuged at 5000 rpm for 30 min; the supernatant was retained.

4.2. Device fabrication

CH_3NH_3I (MAI) was synthesized as reported elsewhere [55]. To prepare the perovskite precursor solution, we mixed MAI and PbI_2 (molar ratio 1:1) powders in anhydrous DMF at concentration 50 mass %. the solution was stirred for more than 4 h at 70 °C and filtered through a polyvinylidene difluoride (PVDF) membrane (0.45 μm) before device fabrication. The devices were fabricated with a p–i–n configuration ITO/GO (GO/Cdots)/$CH_3NH_3PbI_3$/PCBM/BCP/Ag. The etched ITO substrates were cleaned and exposed to ultraviolet light and O_3 for 18 min. A GO solution (1 mg/mL in DMF, synthesized according to the method of Hummers explained in a previous report [25]) was spin-coated onto the substrates at 4000 rpm for 40 s. after annealing at 120 °C for 15 min, the substrates were transferred into a glove box for subsequent deposition of perovskite and an electron-transport layer. Before perovskite deposition, Cdots_CB solutions (concentrations 0.025, 0.05 and 0.1 mg/mL in chlorobenzene) were spin-coated on the GO film at 3000 rpm for 30 s and annealed at 60 °C for 5 min. These films as prepared are labeled here as GO/Cdots_0.025, GO/Cdots_0.05 and GO/Cdots_0.1, respectively. The perovskite precursor solution was dripped onto the ITO/GO (GO/Cdots) substrate spinning at a rate of 5000 rpm. the total duration of spin-coating was 15 s; chlorobenzene serving as antisolvent was injected onto the substrate after spinning 5 s. the perovskite film was then annealed at 100 °C for 2 min; the samples were treated with solvent annealing technique under DMF vapor for 10 min at the same temperature. Afterward, Methanofullerene phenyl-C61-butyric-acid-Methyl-ester (PCBM, 20 mg, FEM Tech) was dissolved in chlorobenzene (1 mL) and spin-coated on top of the perovskite layer at 1000 rpm for 30 s. bathocuproine (BCP) (concentration 0.5 mg/mL in isopropyl alcohol, IPA) was spin-coated at 400 rpm on top of the PCBM layer. The silver back-contact electrode (100 nm) was eventually deposited via thermal evaporation in a vacuum chamber

4.3. Preparation of a Cdots UV-to-Vis downshifting layer

The Cdots dispersed in isopropanol were mixed with polyvinylpyrrolidone (PVP) polymer (final concentration 200 mg/mL). The concentration of Cdots was about 2 mg/mL. The solution was then spin-coated at 800 rpm for 30 s on the back side of an assembled PSC (thickness 50–100 μm). Before spin-coating, the active area was protected with a tape.

4.4. Characterization of materials and devices

The current–voltage characteristics were measured with a digital source meter (Keithley 2400) with the device under one-sun illumination (AM 1.5G, 100 mW cm^{-2}) from a solar simulator (XES-40S1, SAN-E1). The spectra of the IPCE of the corresponding devices were recorded with a system consisting of a Xe lamp (PTiA-1010, 150W), a monochromator (PTi, containing a grating with 1200 g mm^{-1} blazed at

500 nm) and a source meter (Keithley 2400). XRD patterns were recorded with an X-ray diffractometer (bruker AXS, D8 Advance, Cu K_α, $\lambda = 1.5418$ Å). A scanning electron microscope (SEM, Hitachi SU-8010) was used to investigate the morphology of the films. Absorption spectra were recorded with a spectrophotometer (JASCO V-570); the PL transient spectra were recorded with a time-correlated single-photon counting (TCSPC) system (Picoharp 300, PicoQuant) with excitation at 635 nm from a picosecond pulsed-diode laser (LDH-635, PicoQuant, FWHM ~70 ps). The rate of repetition of the laser used for all experiments was 25 MHz; the pulse energy per unit area was 4 μJ cm-2. The PL temporal profiles were collected at 770 ± 16 nm, using a microchannel-plate photomultiplier tube (MCP-PMT, R3809U-50). Transient open-circuit photovoltage (TPV) decays were measured with a home-built setup. The sample was biased under a white-light light-emitting diode (LED, HP-HC30W3, Createk) at varied intensities; a small perturbation was introduced with a blue LED (HP-HC30B3, Createk) modulated at 1 kHz with a function generator (AFG-2225, GW Instek). The VOC transient decay was recorded with an oscilloscope (HDO 4034, Teledyne Lecroy)

Cyclic voltammetric (CV) measurements were performed under N_2 with a Ag/AgCl reference electrode, a Au disc as working electrode and a Pt foil as auxiliary electrode in a computer-controlled electrochemistry system (Solartron 1087). Before use, the working electrode was polished with alumina powder (1, 0.3, 0.1 μm), rinsed with copious amounts of water (Milli-Q), and cleaned electrochemically with H_2SO_4 (0.5 M) with electrolyte tetrabutylammonium perchlorate (TBAP, 0.1 M in acetonitrile). Before use, TBAP was dried *in vacuum* for at least 4 h at 80 °C. Cdots (5 μL) were dried on the Au electrode; CV was performed in a potential window [-2.5 V; +2.5 V] at scan rate 5 mV/s. The HOMO/LUMO of the Cdots were calculated using the following formula:

$$E(HOMO) = -(E_{ox,onset} + E_{vac,ferrocene} - E_{redox,ferrocene})$$

$$E(LUMO) = -(E_{red,onset} + E_{vac,ferrocene} - E_{redox,ferrocene})$$

These potentials are relative to a Ag/AgCl reference electrode; $E_{vac,ferrocene}$ is taken equal to 4.8 eV; $E_{redox,ferrocene}$ was calculated to be 0.42 V vs Ag/AgCl [56,57].

Acknowledgments

D.B. acknowledges financial support for his visit to NCTU from the joint program Summer Institute in Taiwan (SIT) from Minister of Science and Technology (MOST) of Taiwan, National Chiao Tung University (Hsinchu, Taiwan) and the Natural Science and Engineering Research Council of Canada (NSERC). This work is supported by MOST, Taiwan (Contract numbers: MOST 107-3017-F009-003; MOST 105-2119-M-009-MY3; MOST 106-2119-M-009-001) and the Center for Emergent Functional Matter Science of National Chiao Tung University from The Featured Areas Research Center Program within the framework of the Higher Education Sprout Project by the Ministry of Education in Taiwan. F.R. is supported by an individual Discovery Grant from NSERC and acknowledges partial salary support from the Canada Research Chairs program. F.R. is also grateful to the government of China for a Chang Jiang short term scholar award and to Sichuan province for a 1000 talent short term award.

References

[1] B. O'Regan, M. Grätzel, Nature 353 (1991) 737.
[2] C.-L. Wang, J.-Y. Hu, C.-H. Wu, H.-H. Kuo, Y.-C. Chang, Z.-J. Lan, H.-P. Wu, E. Wei-Guang Diau, C.-Y. Lin, Energy Environ. Sci. 7 (2014) 1392–1396.
[3] A. Yella, H.-W. Lee, H.N. Tsao, C. Yi, A.K. Chandiran, M.K. Nazeeruddin, E.W.-G. Diau, C.-Y. Yeh, S.M. Zakeeruddin, M. Grätzel, Science 334 (2011) 629–634.
[4] C.-C. Chen, W.-H. Chang, K. Yoshimura, K. Ohya, J. You, J. Gao, Z. Hong, Y. Yang, Adv. Mater. 26 (2014) 5670–5677.
[5] J. You, L. Dou, K. Yoshimura, T. Kato, K. Ohya, T. Moriarty, K. Emery, C.-C. Chen, J. Gao, G. Li, Y. Yang, Nat. Commun. 4 (2013) 1446.
[6] G.S. Selopal, H. Zhao, X. Tong, D. Benetti, F. Navarro-Pardo, Y. Zhou, D. Barba, F. Vidal, Z.M. Wang, F. Rosei, Adv. Funct. Mater. 27 (2017) 1701468.
[7] Z. Yang, J.Z. Fan, A.H. Proppe, F.P.G.d. Arquer, D. Rossouw, O. Voznyy, X. Lan, M. Liu, G. Walters, R. Quintero-Bermudez, B. Sun, S. Hoogland, G.A. Botton, S.O. Kelley, E.H. Sargent, Nat. Commun. 8 (2017) 1325.
[8] M. Grätzel, Acc. Chem. Res. 50 (2017) 487–491.
[9] J.M. Ball, M.M. Lee, A. Hey, H.J. Snaith, Energy Environ. Sci. 6 (2013) 1739.
[10] T. Liu, K. Chen, Q. Hu, R. Zhu, Q. Gong, Adv. Energy Mater. 6 (2016) 1600457.
[11] K. Mahmood, S. Sarwar, M.T. Mehran, RSC Adv. 7 (2017) 17044–17062.
[12] Z.H. Bakr, Q. Wali, A. Fakharuddin, L. Schmidt-Mende, T.M. Brown, R. Jose, Nano Energy 34 (2017) 271–305.
[13] L. Calió, S. Kazim, M. Grätzel, S. Ahmad, Angew. Chem. Int. Ed. 55 (2016) 14522–14545.
[14] C. Sun, Z. Wu, H.L. Yip, H. Zhang, X.F. Jiang, Q. Xue, Z. Hu, Z. Hu, Y. Shen, M. Wang, Advanced Energy Materials 6 (2016) 1501534.
[15] L. Tian, Z. Hu, X. Liu, Z. Liu, P. Guo, B. Xu, Q. Xue, H.-L. Yip, F. Huang, Y. Cao, ACS Appl. Mater. Interfaces 11 (2019) 5289–5297.
[16] S.N. Habisreutinger, T. Leijtens, G.E. Eperon, S.D. Stranks, R.J. Nicholas, H.J. Snaith, Nano Lett. 14 (2014) 5561–5568.
[17] G. Yang, H. Tao, P. Qin, W. Ke, G. Fang, J. Mater. Chem. 4 (2016) 3970–3990.
[18] M. Acik, S.B. Darling, J. Mater. Chem. 4 (2016) 6185–6235.
[19] D. Benetti, K.T. Dembele, J. Benavides, H. Zhao, S. Cloutier, I. Concina, A. Vomiero, F. Rosei, J. Mater. Chem. C 4 (2016) 3555–3562.
[20] K.T. Dembele, G.S. Selopal, R. Milan, C. Trudeau, D. Benetti, A. Soudi, M.M. Natile, G. Sberveglieri, S. Cloutier, I. Concina, F. Rosei, A. Vomiero, J. Mater. Chem. 3 (2015) 2580–2588.
[21] S.-S. Li, K.-H. Tu, C.-C. Lin, C.-W. Chen, M. Chhowalla, ACS Nano 4 (2010) 3169–3174.
[22] J.-M. Yun, J.-S. Yeo, J. Kim, H.-G. Jeong, D.-Y. Kim, Y.-J. Noh, S.-S. Kim, B.-C. Ku, S.-I. Na, Adv. Mater. 23 (2011) 4923–4928.
[23] Z. Yu, L. Sun, Advanced Energy Materials 5 (2015) 1500213.
[24] C.-C. Chung, S. Narra, E. Jokar, H.-P. Wu, E. Wei-Guang Diau, J. Mater. Chem. 5 (2017) 13957–13965.
[25] E. Jokar, Z.Y. Huang, S. Narra, C.-Y. Wang, V. Kattoor, C.-C. Chung, E.W.-G. Diau, Adv. Energy Mater. 8 (2018) 1701640.
[26] K. Aitola, K. Sveinbjornsson, J.-P. Correa-Baena, A. Kaskela, A. Abate, Y. Tian, E.M.J. Johansson, M. Gratzel, E.I. Kauppinen, A. Hagfeldt, G. Boschloo, Energy Environ. Sci. 9 (2016) 461–466.
[27] S.S. Bhosale, E. Jokar, A. Fathi, C.M. Tsai, C.Y. Wang, E.W.G. Diau, Adv. Funct. Mater. 28 (2018) 1803200..
[28] V. Georgakilas, J.A. Perman, J. Tucek, R. Zboril, Chem. Rev. 115 (2015) 4744–4822.
[29] S.Y. Lim, W. Shen, Z. Gao, Chem. Soc. Rev. 44 (2015) 362–381.
[30] H. Li, W. Shi, W. Huang, E.-P. Yao, J. Han, Z. Chen, S. Liu, Y. Shen, M. Wang, Y. Yang, Nano Lett. 17 (2017) 2328–2335.
[31] Z. Jia, Y. Yue, L. Gaolin, Y. Shu-Hong, Adv. Sci. 2 (2015) 1500002.
[32] W.S. Yang, B.-W. Park, E.H. Jung, N.J. Jeon, Y.C. Kim, D.U. Lee, S.S. Shin, J. Seo, E.K. Kim, J.H. Noh, S.I. Seok, Science 356 (2017) 1376–1379.
[33] National Renewable Energy Laboratory, National Renewable Energy Laboratory (NREL), (2018).
[34] M.A. Green, A. Ho-Baillie, H.J. Snaith, Nat. Photon. 8 (2014) 506–514.
[35] M.M. Lee, J. Teuscher, T. Miyasaka, T.N. Murakami, H.J. Snaith, Science 338 (2012) 643–647.
[36] Z. Wu, S. Bai, J. Xiang, Z. Yuan, Y. Yang, W. Cui, X. Gao, Z. Liu, Y. Jin, B. Sun, Nanoscale 6 (2014) 10505–10510.
[37] Q. Guo, F. Yuan, B. Zhang, S. Zhou, J. Zhang, Y. Bai, L. Fan, T. Hayat, A. Alsaedi, Z.a. Tan, Nanoscale 11 (2019) 115–124.
[38] Y. Ma, H. Zhang, Y. Zhang, R. Hu, M. Jiang, R. Zhang, H. Lv, J. Tian, L. Chu, J. Zhang, ACS Appl. Mater. Interfaces 11 (2018) 3044–3052.
[39] J. Jin, C. Chen, H. Li, Y. Cheng, L. Xu, B. Dong, H. Song, Q. Dai, ACS Appl. Mater. Interfaces 9 (2017) 14518–14524.
[40] S. Kasi Matta, C. Zhang, A.P. O'Mullane, A. Du, ChemPhysChem : Eurp. J. Chem. Phys. Phys. Chem. 19 (2018) 3018–3023.
[41] Y. Rong, L. Liu, A. Mei, X. Li, H. Han, Adv. Energy Mater. 5 (2015) 1501066-n/a.
[42] W. Li, W. Zhang, S. Van Reenen, R.J. Sutton, J. Fan, A.A. Haghighirad, M.B. Johnston, L. Wang, H.J. Snaith, Energy Environ. Sci. 9 (2016) 490–498.
[43] Y. Zhou, D. Benetti, X. Tong, L. Jin, Z.M. Wang, D. Ma, H. Zhao, F. Rosei, Nano Energy 44 (2018) 378–387.
[44] M. Fu, F. Ehrat, Y. Wang, K.Z. Milowska, C. Reckmeier, A.L. Rogach, J.K. Stolarczyk, A.S. Urban, J. Feldmann, Nano Lett. 15 (2015) 6030–6035.
[45] H. Ding, J.-S. Wei, N. Zhong, Q.-Y. Gao, H.-M. Xiong, Langmuir : ACS J. Surface Colloids 33 (2017) 12635–12642.
[46] X. Dong, Y. Su, H. Geng, Z. Li, C. Yang, X. Li, Y. Zhang, J. Mater. Chem. C 2 (2014) 7477–7481.
[47] A. Privitera, M. Righetto, D. Mosconi, F. Lorandi, A.A. Isse, A. Moretto, R. Bozio, C. Ferrante, L. Franco, Phys. Chem. Chem. Phys. 18 (2016) 31286–31295.
[48] P. Yu, X. Wen, Y.-R. Toh, Y.-C. Lee, K.-Y. Huang, S. Huang, S. Shrestha, G. Conibeer, J. Tang, J. Mater. Chem. C 2 (2014) 2894–2901.
[49] D. Shi, V. Adinolfi, R. Comin, M. Yuan, E. Alarousu, A. Buin, Y. Chen, S. Hoogland, A. Rothenberger, K. Katsiev, Y. Losovyj, X. Zhang, P.A. Dowben, O.F. Mohammed, E.H. Sargent, O.M. Bakr, Science 347 (2015) 519–522.

[50] N.F. Montcada, J.M. Marín-Beloqui, W. Cambarau, J. Jiménez-López, L. Cabau, K.T. Cho, M.K. Nazeeruddin, E. Palomares, ACS Energy Letters 2 (2017) 182–187.
[51] A. Guerrero, G. Garcia-Belmonte, I. Mora-Sero, J. Bisquert, Y.S. Kang, T.J. Jacobsson, J.-P. Correa-Baena, A. Hagfeldt, J. Phys. Chem. C 120 (2016) 8023–8032.
[52] A. Pockett, G.E. Eperon, T. Peltola, H.J. Snaith, A. Walker, L.M. Peter, P.J. Cameron, J. Phys. Chem. C 119 (2015) 3456–3465.
[53] D. Benetti, D. Cui, H. Zhao, F. Rosei, A. Vomiero, Small 14 (2018) 1801668.
[54] S. Qu, X. Liu, X. Guo, M. Chu, L. Zhang, D. Shen, Adv. Funct. Mater. 24 (2014) 2689–2695.
[55] J. Qiu, Y. Qiu, K. Yan, M. Zhong, C. Mu, H. Yan, S. Yang, Nanoscale 5 (2013) 3245–3248.
[56] V.V. Pavlishchuk, A.W. Addison, Inorg. Chim. Acta 298 (2000) 97–102.
[57] R.R. Gagne, C.A. Koval, G.C. Lisensky, Inorg. Chem. 19 (1980) 2854–2855.